Site-Selective Deposition of In 2 O 3 Using a Self-Assembled Monolayer

ARTICLE *in* CRYSTAL GROWTH & DESIGN · JANUARY 2009

Impact Factor: 4.89 · DOI: 10.1021/cg800856m

3 AUTHORS, INCLUDING:

Yoshitake Masuda
National Institute of Advanced Industrial S…
305 PUBLICATIONS **5,409** CITATIONS

Article

Site-Selective Deposition of InO Using a Self-Assembled Monolayer

Yoshitake Masuda, Masashi Kondo, and Kunihito Koumoto

Cryst. Growth Des., **2009**, 9 (1), 555-561• DOI: 10.1021/cg800856m • Publication Date (Web): 26 November 2008

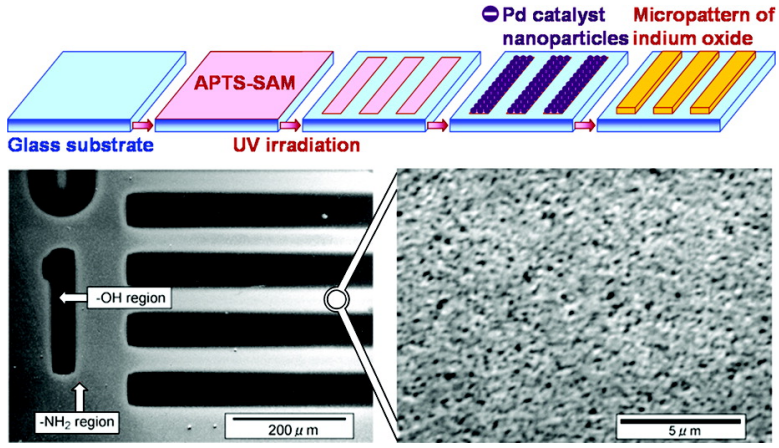

More About This Article

Additional resources and features associated with this article are available within the HTML version:

- Supporting Information
- Access to high resolution figures
- Links to articles and content related to this article
- Copyright permission to reproduce figures and/or text from this article

View the Full Text HTML

CRYSTAL GROWTH & DESIGN
2009
VOL. 9, NO. 1
555–561

Site-Selective Deposition of In_2O_3 Using a Self-Assembled Monolayer

Yoshitake Masuda,*[,†,‡] Masashi Kondo,[‡] and Kunihito Koumoto[†]

National Institute of Advanced Industrial Science and Technology (AIST), 2266-98 Anagahora, Shimoshidami, Moriyama-ku, Nagoya 463-8560, and Graduate School of Engineering, Nagoya University, Nagoya 464-8603, Japan

Received August 5, 2008; Revised Manuscript Received October 1, 2008

ABSTRACT: We developed a micropattern of transparent conducting In_2O_3 thin films in an aqueous solution without an etching process. Molecular recognition of a self-assembled monolayer was effectively utilized for site-selective deposition of In_2O_3 thin films. This novel system allowed us to realize liquid-phase patterning of transparent conducting In_2O_3 thin films without degradation of its high performance in the etching process. Indium ions in the residual solution can be used for In_2O_3 film formation repeatedly. Indium feedstock can be transformed to In_2O_3 in a 100% yield. This process also has the advantage of green chemistry such as an environmentally friendly process, ordinary temperature process, and atmospheric pressure process, without the use of a toxic acid etchant. The process offers a novel direction for the design of future materials and devices with high performance and environmental harmony.

Introduction

In_2O_3, an important transparent conducting oxide (TCO) material with a wide energy band gap (direct band gap of about 3.6 eV and indirect band gap of about 2.6 eV) possessing unusually high electrical conductivity and optical transparency (>70%) in the visible region, has been widely exploited in many applications such as optoelectronic devices,[1] organic/polymer light-emitting diodes (O/PLEDs), solar cells,[2−4] flat-panel liquid-crystal displays (LCDs),[5,6] grating materials,[7] electrochromic devices,[8] and ultrasensitive gas sensors for detection of O_3,[9] CO_2,[10] H_2,[10,11] NO_2,[11] and Cl_2.[12]

Thin films of In_2O_3 can be prepared by a variety of techniques such as rf and dc sputtering,[13] vacuum and e-beam evaporation,[14,15] thermal oxidation,[16,17] reactive ion plating,[18] the sol−gel technique,[19] reactive evaporation,[20] CVD,[21,22] ultrasonic spray CVD,[23] spray pyrolysis,[24,25] and laser ablation.[26]

For patterning of TCO thin films such as In_2O_3 or Sn-doped In_2O_3 (ITO), either dry etching or wet etching can be adopted to produce the fine patterns.[5] Wet etching is a simpler process than dry etching and has a high throughput and low cost, and so is often used to pattern these films in the panel industry. The wet etching processes, however, might cause problems of selective grain-boundary etching and isotropic etching, and the existing In_2O_3 or ITO deposition methods also tend to generate different etching rates.[27] Such nonuniform etching phenomena worsen the electrical properties of the TCO electrode and might lead to serious undercut phenomena.[28]

The wet etching characteristics of In_2O_3 or ITO are highly dependent on the microstructure and microcrystallinity of the film itself; small variations in the films could leave residues after etching and also could cause the sidewall consumption of TCO thin films.[29,30] Additionally, In_2O_3 and ITO can only be dissolved in acidic solutions,[31−33] and thus, conventional etchants are generally composed of strong acids, such as halogen acid,[34,35] and aqua regia.[28] For the widely used top-ITO structures in LCD, corrosion of the underlayer metal is serious during patterning of ITO films using strong acids,[36] and the residual halide also degrades devices.[28] Therefore, preparation of uniform TCO thin films and a novel patterning process which involves no etching process are strongly needed for high-performance nano/micro TCO devices.

Recently, site-selective deposition of oxide films was proposed, and nano/microfabrication such as 2D patterning of oxide films was realized utilizing self-assembled monolayers (SAMs).[37−40] Molecular recognition, chemical reaction, and various functions of organic head groups of SAMs were effectively applied for control of nucleation, growth, and deposition of oxide materials on the basis of scientific knowledge about the deposition mechanism[41] and interface phenomena. Nano/micropatterning of TiO_2 thin films having a 200 nm line width, a 100 nm interval, and a 70 nm thickness was realized with the site-selective deposition, which is the finest pattern achieved in the solution,[42] and micropatterning of various oxides has been developed.[43−47] In this study, we attempted to apply a high-performance SAM for micropatterning of transparent conducting In_2O_3 thin films.

Here, we propose a novel process to prepare uniform transparent conducting In_2O_3 thin films and realize micropatterning of In_2O_3 thin films in an aqueous solution without an etching process. Molecular recognition of a self-assembled monolayer was effectively utilized for site-selective deposition of In_2O_3 thin films. This novel system allowed us to realize liquid-phase patterning of transparent conducting In_2O_3 thin films without degradation of its high performance in the etching process. This process also has the advantage of green chemistry such as an environmentally friendly process, ordinary temperature process, and atmospheric pressure process, without the use of a toxic acid etchant. The process offers a novel direction for the design of future materials and devices with high performance and environmental harmony.

Experimental Section

SAM Preparation and Its Modification. The glass substrate was cleaned ultrasonically in acetone, ethanol, and deionized water for 5 min in this order and was exposed to ultraviolet light and ozone gas for 10 min to remove organic contamination by using a UV/ozone cleaner (184.9 and 253.7 nm) (low-pressure mercury lamp 200 W, PL21-200, SEN Lights Co., 18 mW/cm^2, distance from lamp 30 mm, 24 °C, humidity 73%, air flow 0.52 m^3/min, 100 V, 320 W).[48−51] An APTS [(3-aminopropyl)triethoxysilane] SAM was prepared by im-

* To whom correspondence should be addressed. E-mail: masuda-y@aist.go.jp.
† AIST.
‡ Nagoya University.

10.1021/cg800856m CCC: $40.75
Published on Web 11/26/2008

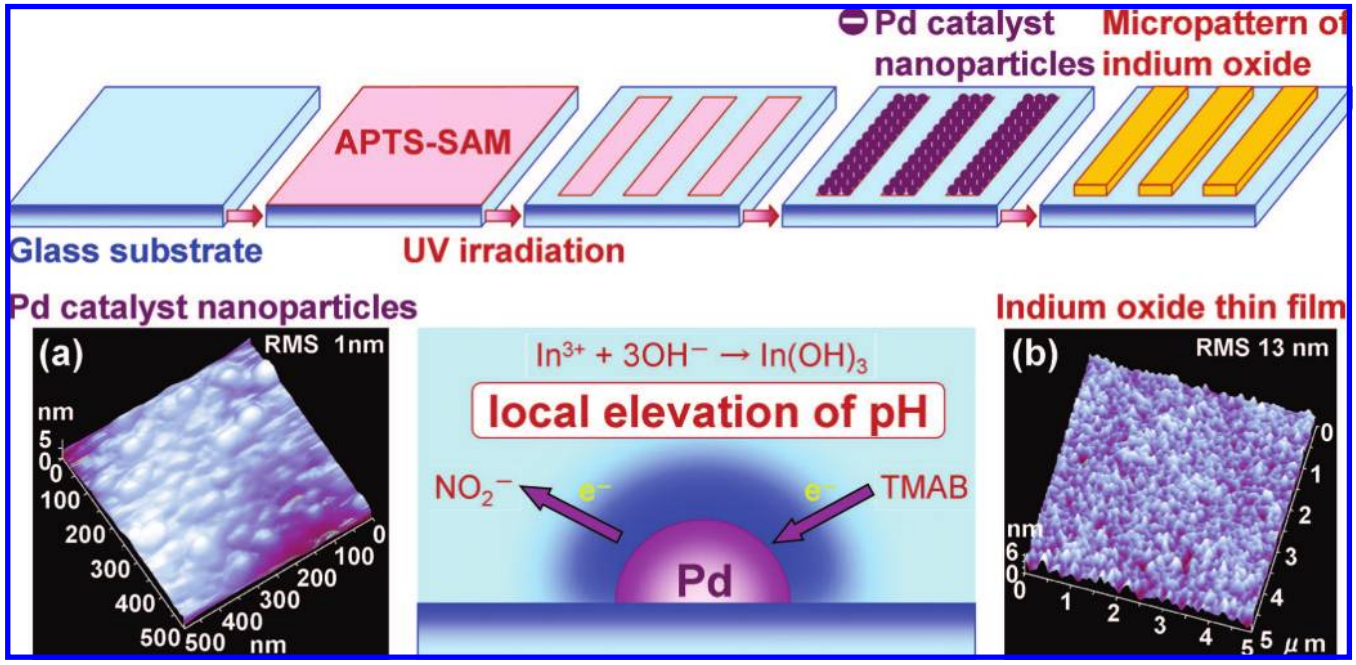

Figure 1. Conceptual process for micropatterning of indium oxide thin films on a glass substrate. AFM images of (a) Pd catalyst nanoparticles and (b) indium oxide thin films (lower stand).

mersing the Si substrate in an anhydrous toluene solution containing 1 vol % APTS for 1 h in a N_2 atmosphere (Figure 1). The substrate was rinsed with fresh anhydrous toluene in a N_2 atmosphere. The substrate with the SAM was baked at 120 °C for 5 min to remove residual solvent and promote chemisorption of the SAM.

The APTS SAM was then irradiated by ultraviolet light (PL21-200) through a photomask (test chart no. 1, N type, quartz substrate, 1.524 mm thickness, guarantee of line width 2 μm $\pm$ 0.5 μm, Toppan Printing Co., Ltd.) for 10 min (Figure 1). UV irradiation modified the amino groups to silanol groups forming a pattern of amino group regions and silanol group regions. The patterned APTS SAM having amino regions and silanol regions was used as a template for patterning of Pd nanoparticles. The initially deposited APTS SAM showed a water contact angle of 48°. UV-irradiated surfaces of the SAM were, however, wetted completely (contact angle <5°). This suggests that the SAM of APTS was modified to hydrophilic OH group surfaces by UV irradiation.

Characterization. The patterned APTS SAM prepared on a glass substrate was immersed in the solution containing Pd nanoparticles (Figure 1). Pd nanoparticles were adsorbed on amino group regions of a patterned SAM by electrostatic interaction between Pd nanoparticles and the APTS SAM. The particle size of the Pd colloids and ζ potential of the Pd nanoparticles, APTS SAM, and silanol SAM were measured by electrophoretic light scattering equipment (ELS-8000, Otsuka Electronics Co., Ltd.). The APTS SAM covered Pd nanoparticles were observed by a scanning probe microscope (SPI 3800N, Seiko Instruments Inc.) that was operated in AFM (atomic force microscopy) tap mode to observe the topography of the surface. AFM scans were operated at room temperature under ambient air. The surface of the patterned APTS SAM covered Pd nanoparticles was further evaluated by X-ray photoelectron spectroscopy (XPS) (ESCALAB 210, VG Scientific Ltd.) in which the X-ray source (Mg Kα, 1253.6 eV) was operated at 15 kV and 18 mA, and the analysis chamber pressure was $(1-3) \times 10^{-7}$ Pa. Site-selective deposition of Pd on a patterned APTS SAM was evaluated as a mapping image by secondary ion mass spectroscopy (SIMS; TOF-SIMS IV, ION-TOF GmbH, 2.4 pA of Ga^+, 25 keV).

The substrate having Pd nanoparticles on amino group regions was then immersed in an aqueous solution containing $In(NO_3)_3$ and TMAB (trimethylamine−borane complex, $(CH_3)_3N-BH_3$, CAS 75-22-9) at 65 °C for 1 h (Figure 1). Indium oxide was deposited on Pd-adsorbed regions to form patterned thin films. After having been immersed in the solution, the substrates were rinsed with distilled water and observed by a scanning electron microscope (S-3000N, Hitachi, Ltd.) and a scanning probe microscope. The distribution of elements on the surface of the substrates was evaluated by an energy-dispersive X-ray (EDX) analyzer (EDAX Falcon, EDAX Co., Ltd.), which is built into the scanning electron microscope. The surface of thin films was further evaluated by XPS. The crystal phase was evaluated by an X-ray diffractometer (RINT-2100, Rigaku) with Cu Kα radiation (40 kV, 30 mA) and a Ni filter plus a graphite monochromator. Transmittance and reflectance of the indium oxide film were evaluated by a UV/vis/NIR spectrophotometer (V-570, JASCO Co., Ltd.) with FLH-467 for transmittance or ARN-475 for reflectance. The optical band gap was estimated from the transmittance and reflectance of the films. The specific resistance (R), carrier concentration (n), and Hall mobility (μ) of indium oxide thin films were evaluated after annealing at 300 °C in a reduced atmosphere (3% H_2/N_2).

Results and Discussion

Synthesis and Patterning of Pd Nanoparticles. A catalyst dispersion[52,53] containing Na_2PdCl_4 (0.38 mM) and NaCl (0.01 M) in a 0.01 M 2-morpholinoethanesulfonate pH 5 aqueous buffer was prepared (Figure 1) as described in refs 52−54. Hydrolyzed Pd colloids were formed in this solution.[53] Light-scattering measurements indicated that the catalyst dispersion contained colloid particles of about 30 nm diameter. Pd nanoparticles showed a negative ζ potential (−30.5 eV) at pH 5. The APTS SAM showed a positive ζ potential at pH 5 because of protonation of the amino group ($-NH_2$) to $-NH_3^+$. Silanol groups of the UV-irradiated APTS SAM, on the other hand, showed a negative ζ potential at pH 5 caused by deprotonation of the silanol group ($-SiOH$) to $-SiO^-$. The patterned APTS SAM was immersed in the colloidal dispersion of catalyst at 25 °C for 30 min, and the catalyzed APTS SAM was rinsed with water. Pd colloids adsorbed on amine groups of the APTS SAM by electrostatic interactions between the negative surface charge of Pd colloids and positive surface charge of the APTS-SAM[45] and formed covalent bonds,[53] while an electrostatic repulsion force kept Pd catalyst particles away from silanol group regions having a negative ζ potential.

Pd nanoparticles deposited on amino group regions of a patterned SAM had a diameter of about 30 nm and a surface

roughness (rms) of about 1 nm as shown by AFM observation (Figure 1). Pd was found to be adsorbed on amino group regions uniformly to form a thin catalytic layer with a small surface roughness. The even application, small thickness, and small surface roughness of the Pd layer are significant for deposition of a uniform transparent indium oxide layer.

Furthermore, site-selective adsorption of Pd was clearly observed by TOF-SIMS mapping.[45] Bright regions due to Pd (m/z = 104, 105, 106, 108, and 110) were observed on the APTS SAM surface, while no Pd signal was seen on the silanol group surface. This result clearly indicates that site-selective adsorption of Pd catalyst occurred on the APTS SAM surface.

Deposition Control of $In(OH)_3$ Thin Films by a Pd Catalyst. The patterned SAM having Pd catalytic nanoparticles on amino group regions was immersed in an aqueous solution containing $In(NO_3)_3$ and TMAB at 65 °C for 1 h (Figure 1). Nitrate ions were generated by dissolution of indium nitrate in water according to

$$In(NO_3)_3 \rightarrow In^{3+} + 3NO_3^- \quad \text{(a)}$$

The Pd catalyst is indispensable for eqs b and c. Oxidation of the reducing agent TMAB is promoted by the Pd catalyst to generate electrons in eq b. Nitrate ions are reduced to nitrite ions by receiving electrons according to eq c. Hydroxide ions are generated by oxidation−reduction reactions near the Pd catalyst according to eq c. Local elevation of the pH thus occurs near Pd catalysts.

$$(CH_3)_3NBH_3 + 2H_2O \rightarrow BO_2^- + (CH_3)_3N + 7H^+ + 6e^- \quad \text{(b)}$$

$$NO_3^- + H_2O + 2e^- \rightarrow NO_2^- + 2OH^- \quad \text{(c)}$$

$In(OH)_3$ nucleates and grows at high pH according to eq d. $In(OH)_3$ is thus deposited in Pd-adsorbed regions of the patterned SAM (Figure 1).

$$In^{3+} + 3OH^- \rightarrow In(OH)_3 \quad \text{(d)}$$

A transparent conducting In_2O_3 thin film is fabricated by annealing at 300 °C in a reduced atmosphere (3% H_2/N_2) for 1 h according to eq e.

$$2In(OH)_3 \rightarrow In_2O_3 + 3H_2O \quad \text{(e)}$$

Liquid-Phase Patterning of $In(OH)_3$ Thin Films. After having been immersed in the solution containing $In(NO_3)_3$ and TMAB, the patterned SAM having Pd catalytic nanoparticles on amino regions was rinsed with distilled water and dried in air. The thin film was clearly shown by scanning electron microscopy (SEM) observation to deposit on amino group regions selectively (Figure 2). Silanol group regions and amino group regions of the SAM were shown to be black or white, respectively. Magnified SEM micrograph b shows the surface morphology of deposited thin films. The thin films were continuous films without micrometer-scale cracks.

The distribution of elements on the surface of the substrates was evaluated by EDX. Indium was detected from thin films on amino group regions selectively and appeared black in EDX

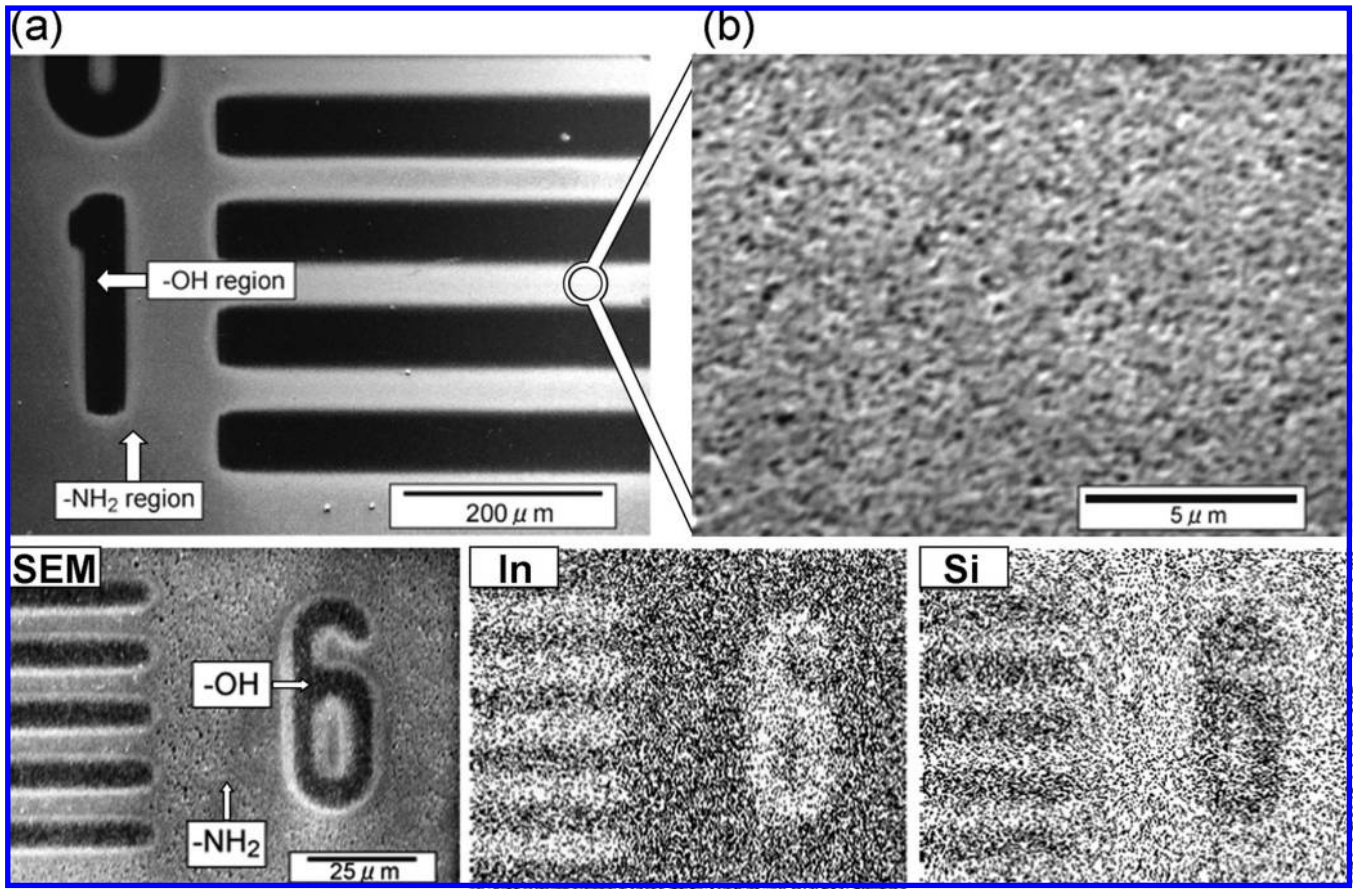

Figure 2. SEM micrographs of (a) the micropattern of indium oxide thin films and (b) a magnified area of (a) (upper stand). SEM micrograph and EDX images for In and Si (lower stand).

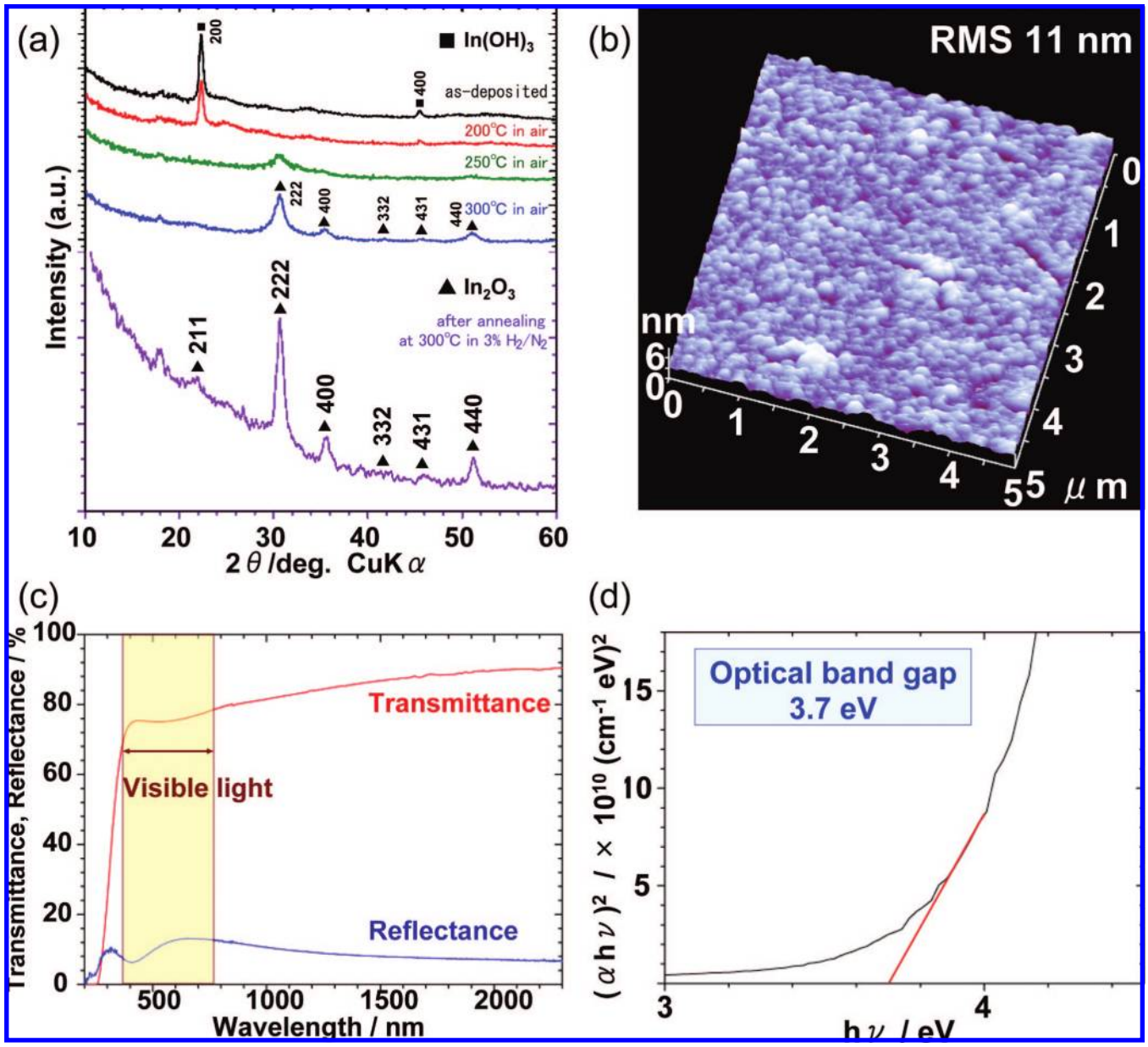

Figure 3. (a) XRD patterns of In_2O_3 thin films before and after annealing at 200, 250, or 300 °C in air for 1 h. XRD pattern of the In_2O_3 thin film after annealing at 300 °C in a reduced atmosphere (3% H_2/N_2) for 1 h. (b) AFM image of the In_2O_3 thin film after annealing at 250 °C. (c) Transmittance and reflectance of the In_2O_3 thin film. (d) Optical band gap estimation of the In_2O_3 thin film.

mapping images (Figure 2). On the other hand, silicon was detected mainly from silanol group regions which were not covered with depositions and exposed bare silicon substrate (Figure 2). These observations showed the site-selective deposition of thin films containing indium on amino group regions.

The surface morphology was further evaluated by AFM conducted at room temperature under ambient air. Thin films were observed on the amino group regions selectively to form microscale patterns. The surface of the thin films showed a uniform morphology and low surface roughness rms = 13 nm (Figure 1). The thin films deposited on a glass substrate were found to be transparent, which would be caused by the low surface roughness, which reduces diffuse reflection. The in-plane particle size was estimated to be about 10−25 nm in diameter. The film thickness at the edge of the thin film was estimated to be 84 nm.

The as-deposited thin film was shown to be crystalline $In(OH)_3$ (JCPDS no. 16-0161) with no additional phase by X-ray diffraction (XRD) evaluation (Figure 3). Only the 002 and 004 diffraction peaks of $In(OH)_3$ were detected. The $In(OH)_3$ thin film was shown to have a high *c*-axis orientation. The crystalline size was estimated to be 17.4 nm by using the 002 diffraction peak. This was consistent with the in-plane particle size estimated by AFM observation. Thus, each particle comprising the thin film would be a single crystal.

Micropatterning of In_2O_3 Thin Films and Their Optical Properties. The $In(OH)_3$ thin film was annealed at 200, 250, and 300 °C in air (Figure 3a). $In(OH)_3$ thin films transformed into single-phase crystalline In_2O_3 above 250 °C. The film annealed at 300 °C showed 222, 400, 332, 431, and 440 diffraction peaks of In_2O_3 (JCPDS no. 44-1087) with no additional phase. The crystalline size was estimated to be 6.8 nm using the 222 diffraction peak, which was about 0.4 times smaller than that of $In(OH)_3$.

Thin films maintained their uniform surface morphology in the annealing at 250 °C in air and showed a low surface

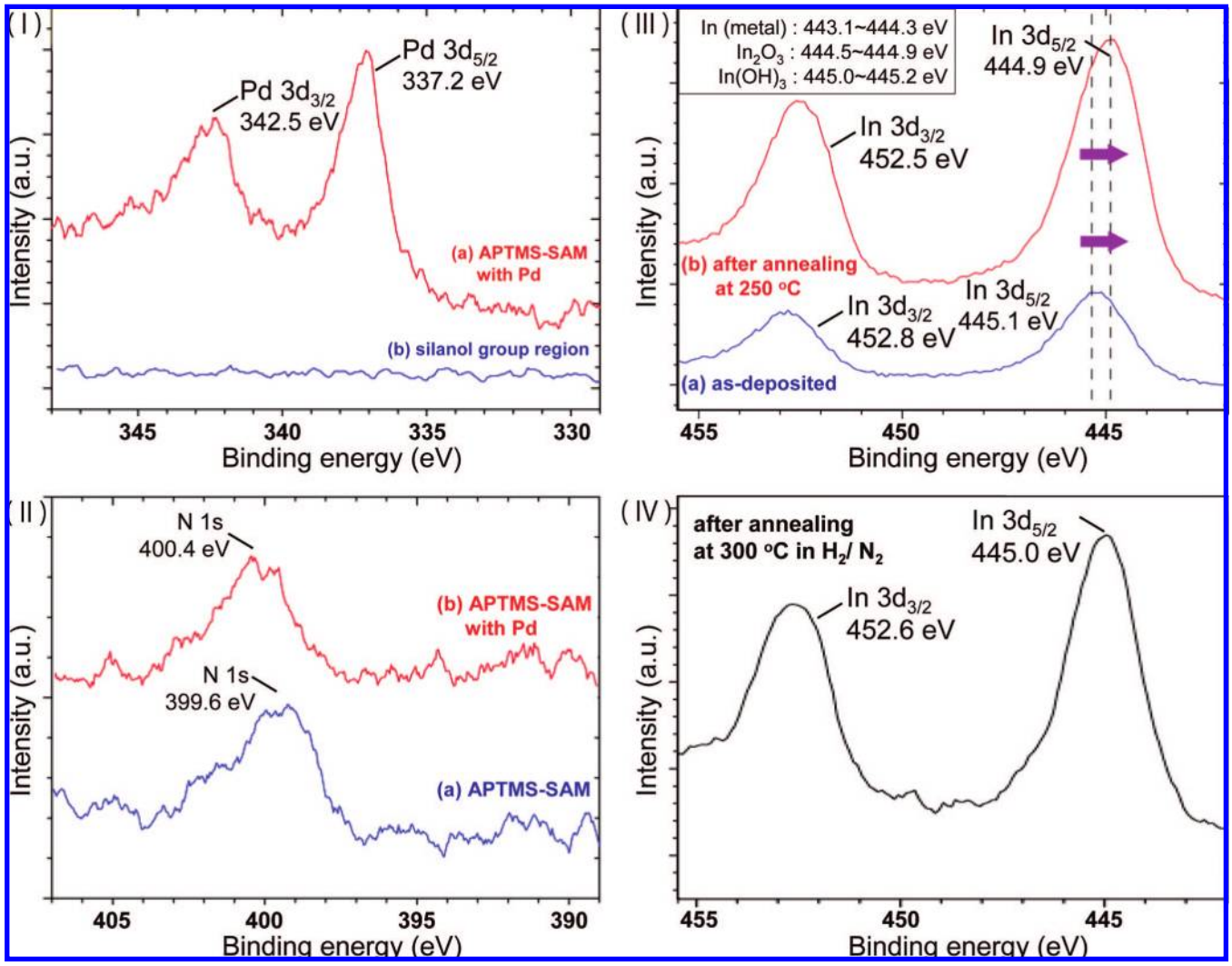

Figure 4. (I) XPS spectra of Pd 3d for the (a) amino group region (APTS SAM) covered with Pd nanoparticles and (b) silanol group region (UV-irradiated APTS SAM) without Pd nanoparticles. (II) XPS spectra of N 1s for the (a) amino group region (APTS SAM) and (b) amino group region (APTS SAM) covered with Pd nanoparticles. (III) XPS spectra of In 3d for indium oxide thin films (a) before and (b) after annealing at 250 °C in air for 1 h. (IV) XPS spectra of In 3d for indium oxide thin films after annealing at 300 °C in a reduced atmosphere (3% H_2/N_2) for 1 h.

roughness rms = 11 nm (Figure 3b). The in-plane particle size was estimated to be about 10−25 nm in diameter. The film thickness on the edge of the thin film was estimated to be 45 nm. Shrinkage of the film thickness would be caused by a volume decrease during crystallization to In_2O_3.

The thin films deposited on a glass substrate showed transparency of 60−70% in the visible light region (Figure 3c), and this would be caused by the low surface roughness, which reduced diffuse reflection to 5−15%.

The optical band gap energy for direct transition in In_2O_3 thin films was estimated to be 3.7 eV assuming that all of the interband transition was direct transition (Figure 3d).

Electrical Property of In_2O_3 Thin Films. The $In(OH)_3$ thin film was annealed at 300 °C in a reduced atmosphere (3% H_2/N_2) for 1 h instead of atmospheric heating to induce oxygen vacancies to increase the carrier concentration. The 222, 400, 332, 431, and 440 diffraction peaks of In_2O_3 (JCPDS no. 44-1087) were observed from the thin film after annealing with no additional phase (Figure 3a). The crystalline size was estimated to be 9.8 nm after annealing at 300 °C in a reduced atmosphere using the 222 diffraction peak, which was about 0.6 times smaller than that of $In(OH)_3$ and slightly larger than that annealed at 300 °C in air.

The carrier concentration and Hall mobility were evaluated to be 2.1×10^{19} cm^{-3} and 5.2 cm^2 V^{-1} s^{-1}, respectively, by Hall effect measurement. The specific resistance was evaluated to be 5.8×10^{-2} Ω cm by the Van der Pauw method. These electrical properties are similar to those of In_2O_3 thin films prepared by the sol−gel method[76] (carrier concentration 1.7×10^{19} cm^{-3}, Hall mobility 5.9 cm^2 V^{-1} s^{-1}, specific resistance 6.1×10^{-2} Ω cm). Electrons would be scattered by grain boundaries in thin films, and this would decrease Hall mobility and increase specific resistance. An increase of the carrier concentration and decrease of grain boundaries by optimization of the reduction conditions and film formation process would allow us to obtain higher Hall mobility and lower specific resistance, thus improving the electrical properties.

XPS Analysis. (a) XPS Analysis for Patterning of Pd Nanoparticles. Pd was detected from amino group regions of a patterned SAM by XPS (Figure 4, panel I). Detection of Pd from amino group regions is consistent with AFM observation, and the deposit observed in the AFM image was shown to be Pd colloid particles. On the other hand, Pd was not observed in silanol regions, i.e., UV-irradiated regions of the APTS SAM, even with XPS, which is a highly surface sensitive analysis method (Figure 4, panel I). Pd adsorption on silanol regions

would be less than the detection limit of XPS. High site selectivity of Pd deposition only on amino group regions of a patterned SAM was shown in XPS analysis.

Pd $3d_{5/2}$ and $3d_{3/2}$ were observed for the APTS SAM at 337.2 and 342.5 eV, respectively (Figure 4, panel I). The binding energy of Pd $3d_{5/2}$ observed is higher than that of Pd metal (334.6 eV,[55] 335.1 eV[56−58]). Referring to an earlier paper,[53] the spectrum of Pd $3d_{5/2}$ can be deconvoluted into three peaks with peak positions corresponding to Pd−N (338.7 eV),[59] Pd−Cl (337.8 eV),[60−62] and Pd−O (336.9 eV)[63] in a Pd−N:Pd−Cl:Pd−O peak ratio of 0.01:0.11:0.88.[45] Pd on the APTS SAM was mainly combined with O as Pd−O (336.9 eV). This result indicates that the surface of the Pd colloid layer on the APTS SAM consists of Pd−O or Pd−OH as well as a small amount of Pd−Cl. Although the Calvert group reported that the hydrolyzed Pd particles form covalent bonds with other SAMs which have amine groups,[53] the Pd−N bond was not observed in our XPS experiment because of the relatively low depth analyzed by the method (the escape depth of the photoelectrons at the binding energy corresponding to Pd $3d_{5/2}$ is a few nanometers), but this does not exclude that Pd−N bonds might have been present also in our case.

N 1s spectra of amino group surfaces were detected before and after the immersion into Pd nanoparticle solution, though the spectrum intensities were very low (Figure 4, panel II). The N 1s binding energy of the amino group surface covered with Pd nanoparticles (400.4 eV) was higher than that before immersion (399.6 eV). The positive shift of N 1s was about 0.8 eV and is similar to that observed between Pd nanoparticles and the amino group of the (3-aminopropyl)triethoxysilane SAM (about 0.8 eV).[64] The shift of N 1s would be caused by the decrease of the electron cloud density around nitrogen atoms and suggests the formation of chemical bonds between nitrogen atoms and Pd ions. The amino group is a strong electron donor and can coordinate to transition-metal ions due to the lone pair electrons of nitrogen atoms. On the other hand, the outermost electron of the soft metal ion Pd(II) is constructed from $4d^8 5s^0 5p^0$ and has an empty lower energy orbit that can accept electrons. Thus, Pd would form strong bonds with nitrogen rather than oxygen and chloride.[64]

(b) XPS Analysis for Patterning of $In(OH)_3$ Thin Films. XPS spectral peaks corresponding to In $3d_{5/2}$ (445.1 eV), In $3d_{3/2}$ (452.8 eV), and O 1s were observed from $In(OH)_3$ thin films deposited on the amino group regions (Figure 4, panel III, curve a).

The binding energy of In $3d_{5/2}$ is higher than those of In metal (443.1 eV,[65] 443.6 eV,[66,67] 443.8 eV,[68] 444.3 eV[69]) and In_2O_3 (444.5 eV,[70,71] 444.6 eV,[72] 444.7 eV,[71,73] 444.8 eV,[67] 444.9 eV[74]), and similar to that of $In(OH)_3$ (445.0 eV,[56] 445.2 eV[75]). This suggests that the indium atoms in thin films are positively charged relative to indium metal by formation of direct bonds with oxygen. The binding energy of In $3d_{5/2}$, which is similar to that of $In(OH)_3$ rather than In_2O_3, is consistent with XRD evaluation. On the other hand, this spectrum was not observed from silanol group regions, revealing site-selective deposition of the $In(OH)_3$ thin film.

(c) XPS Analysis for Patterning of In_2O_3 Thin Films. The spectral peak corresponding to In $3d_{5/2}$ was shifted to a lower binding energy, 444.9 eV, by annealing at 250 °C in air (Figure 4, spectrum III, curve b). This was within the range of that of In_2O_3 and consistent with crystallization into In_2O_3 revealed by XRD evaluation.

Additionally, the $In(OH)_3$ thin film was annealed at 300 °C in a reduced atmosphere (3% H_2/N_2) for 1 h instead of atmospheric heating. In $3d_{5/2}$ was shifted to a lower binding energy, 445.0 eV. This was similar to the binding energy of $3d_{5/2}$ in In_2O_3 and indicated crystallization of $In(OH)_3$ into In_2O_3.

Conclusions

A transparent conducting In_2O_3 circuit was fabricated on a glass substrate using SAMs in an aqueous solution. Micropatterning of In_2O_3 thin films was successfully achieved with self-assembly, without an etching process which deteriorates the performance of the film. Indium ions in the residual solution can be used for In_2O_3 film formation repeatedly. Indium feedstock can be transformed to In_2O_3 in a 100% yield. In_2O_3 thin films showed high transparency (60−70% in the visible light region) and low specific resistance (5.8×10^{-2} Ω cm). The process can also be used to fabricate flexible high-performance TCO devices on polymers such as polyimide. The process offers a novel direction for designing future materials and devices with high performance and environmental harmony.

References

(1) Hambergend, I.; Granquist, C. G. *J. Appl. Phys.* **1996**, 123–160.
(2) Bellingham, J. R.; Mackenize, A. P.; Philips, W. A. *Appl. Phys. Lett.* **1991**, *58*, 2506–2508.
(3) Zhao, L.; Zhou, Z.; Peng, H.; Cui, R. *Appl. Surf. Sci.* **2005**, *252*, 385–392.
(4) Jana, A. K. *J. Photochem. Photobiol., A* **2000**, *132*, 1–17.
(5) Tsai, T. H.; Wu, Y. F. *J. Electrochem. Soc.* **2006**, *153*, C86−C90.
(6) Ozasa, K.; Ye, T.; Aoyagi, Y. *Thin Solid Films* **1994**, *246*, 58–64.
(7) Pissadakis, S.; Mailis, S.; Reekie, L.; Wilkinson, J. S.; Eason, R. W.; Vainos, N. A.; Moschovis, K.; Kiriakidis, G. *Appl. Phys. A: Mater. Sci. Process.* **1999**, *69*, 333–336.
(8) Granqvist, C. G. *Appl. Phys. A: Mater. Sci. Process.* **1993**, *57*, 19–24.
(9) Gagaoudakis, E.; Bender, M.; Douloufakis, E.; Katsarakis, N.; Natsakou, E.; Cimalla, V.; Kiriakidis, G. *Sens. Actuators, B* **2001**, *80*, 155–161.
(10) Chung, W.-Y.; Sakai, G.; Shimanoe, K.; Miura, N.; Lee, D.-D.; Yamazoe, N. *Sens. Actuators, B* **1998**, *46*, 139–145.
(11) Liess, M. *Thin Solid Films* **2002**, *410*, 183–187.
(12) Tamaki, J.; Naruo, C.; Yamamoto, Y.; Matsuoka, M. *Sens. Actuators, B* **2002**, *83*, 190–194.
(13) Ryzhikov, A. S.; Vasiliev, R. B.; Rumyantseva, M. N.; Ryabova, L. I.; Dosovitsky, G. A.; Gilmutdinov, A. M.; Kozlovsky, V. F.; Gaskov, A. M. *Mater. Sci. Eng., B* **2002**, *96*, 268–274.
(14) Murali, K. R.; Sambasivam, V.; Jayachandran, M.; Chockalingam, M. J.; Rangarajan, N.; Venkatesan, V. K. *Surf. Coat. Technol.* **1988**, *35*, 207–213.
(15) Sheu, J. K.; Su, Y. K.; Chi, G. C.; Jou, M. J.; Chang, C. M. *Appl. Phys. Lett.* **1998**, *72*, 3317–3319.
(16) Girtan, M.; Rusu, G. I.; Rusu, G. G.; Gurlui, S. *Appl. Surf. Sci.* **2000**, *162*, 492–498.
(17) Girtan, M.; Rusu, G. I.; Rusu, G. G. *Mater. Sci. Eng., B* **2000**, *76*, 156–160.
(18) Jeong, J. I.; Moon, J. H.; Hong, J. H.; Kang, J.-S.; Fukuda, Y.; Lee, Y. P. *J. Vac. Sci. Technol., A* **1996**, *14*, 293–298.
(19) Gurlo, A.; Ivanovskaya, M.; Pfau, A.; Weimar, U.; Gopel, W. *Thin Solid Films* **1997**, *307*, 288–293.
(20) Korobov, V.; Leibovitch, M.; Shapira, Y. *Appl. Phys. Lett.* **1994**, *65*, 2290–2292.
(21) Maruyama, T.; Fukui, K. *J. Appl. Phys.* **1991**, *70*, 3848–3851.
(22) Maruyama, T.; Kitamura, T. *Jpn. J. Appl. Phys.* **1989**, *28*, 1096–L1097.
(23) Girtan, M. *Surf. Coat. Technol.* **2004**, *184*, 219–224.
(24) Manifacier, J. C.; Fillard, J. P.; Bind, J. M. *Thin Solid Films* **1981**, *77*, 67–80.
(25) Girtan, M.; Cachet, H.; Rusu, G. I. Proceedings of Symposium K on Thin Film Materials for Large Area Electronics of the European Materials Research Society (E-MRS) 2002 Spring Conference. *Thin Solid Films* **2003**, *427*, 406–410.
(26) Grivas, C.; Gill, D. S.; Mailis, S.; Boutsikaris, L.; Vainos, N. A. *Appl. Phys. A: Mater. Sci. Process.* **1998**, *66*, 201–204.
(27) Park, J. Y.; Kim, H. S.; Lee, D. H.; Kwon, K. H.; Yeom, G. Y. *Surf. Coat. Technol.* **2000**, *131*, 247–251.

(28) Huang, C. J.; Su, Y. K.; Wu, S. L. *Mater. Chem. Phys.* **2004**, *84*, 146–150.
(29) van den Meerakker, J. E. A. M.; Baarslag, P. C.; Walrave, W.; Vink, T. J.; Daams, J. L. C. *Thin Solid Films* **1995**, *266*, 152–156.
(30) Takabatake, M.; Wakui, Y.; Konishi, N. *J. Electrochem. Soc.* **1995**, *142*, 2470–2473.
(31) Bradshaw, G.; Hughes, A. J. *Thin Solid Films* **1976**, *33*, L5−L8.
(32) Inoue, M.; Matsuoka, T.; Fujita, Y.; Abe, *Jpn. J. Appl. Phys.* **1989**, *28*, 274–278.
(33) van den Meerakker, J. E. A. M.; ter Veen, W. R. *J. Electrochem. Soc.* **1992**, *139*, 385–390.
(34) Scholten, M.; van den Meerakker, J. E. A. M. *J. Electrochem. Soc.* **1993**, *140*, 471.
(35) Vandenmeerakker, J.; Baarslag, P. C.; Scholten, M. *J. Electrochem. Soc.* **1995**, *142*, 2321–2325.
(36) Takatsuji, H.; Hiromori, T.; Tsujimoto, K.; Tsuji, S.; Kuroda, K.; Saka, H. *Mater. Res. Soc. Symp. Proc.* **1998**, *508*, 315.
(37) Masuda, Y.; Sugiyama, T.; Lin, H.; Seo, W. S.; Koumoto, K. *Thin Solid Films* **2001**, *382*, 153–157.
(38) Masuda, Y.; Jinbo, Y.; Yonezawa, T.; Koumoto, K. *Chem. Mater.* **2002**, *14*, 1236–1241.
(39) Masuda, Y.; Sugiyama, T.; Koumoto, K. *J. Mater. Chem.* **2002**, *12*, 2643–2647.
(40) Masuda, Y.; Ieda, S.; Koumoto, K. *Langmuir* **2003**, *19*, 4415–4419.
(41) Masuda, Y.; Sugiyama, T.; Seo, W. S.; Koumoto, K. *Chem. Mater.* **2003**, *15*, 2469–2476.
(42) Masuda, Y.; Saito, N.; Hoffmann, R.; De Guire, M. R.; Koumoto, K. *Sci. Technol. Adv. Mater.* **2003**, *4*, 461–467.
(43) Shirahata, N.; Masuda, Y.; Yonezawa, T.; Koumoto, K. *Langmuir* **2002**, *18*, 10379–10385.
(44) Saito, N.; Haneda, H.; Sekiguchi, T.; Ohashi, N.; Sakaguchi, I.; Koumoto, K. *Adv. Mater.* **2002**, *14*, 418–421.
(45) Nakanishi, T.; Masuda, Y.; Koumoto, K. *Chem. Mater.* **2004**, *16*, 3484–3488.
(46) Gao, Y. F.; Masuda, Y.; Yonezawa, T.; Koumoto, K. *Chem. Mater.* **2002**, *14*, 5006–5014.
(47) Xiang, J. H.; Masuda, Y.; Koumoto, K. *Adv. Mater.* **2004**, *16*, 1461–1464.
(48) Masuda, Y.; Itoh, T.; Koumoto, K. *Adv. Mater.* **2005**, *17*, 841–845.
(49) Masuda, Y.; Itoh, T.; Koumoto, K. *Langmuir* **2005**, *21*, 4478–4481.
(50) Masuda, Y.; Itoh, T.; Itoh, M.; Koumoto, K. *Langmuir* **2004**, *20*, 5588–5592.
(51) Masuda, Y.; Tomimoto, K.; Koumoto, K. *Langmuir* **2003**, *19*, 5179–5183.
(52) Dressick, W. J.; Kondracki, L. M.; Chen, M. S.; Brandow, S. L.; Matijevic, E.; Calvert, J. M. *Colloids Surf., A* **1996**, *108*, 101 111.
(53) Dressick, W. J.; Dulcey, C. S.; Georger, J. H.; Calabrese, G. S.; Calvert, J. M. *J. Electrochem. Soc.* **1994**, *141*, 210–220.
(54) Brandow, S. L.; Dressick, W. J.; Marrian, C. R. K.; Chow, G. M.; Calvert, J. M. *J. Electrochem. Soc.* **1995**, *142*, 2233–2243.
(55) Hilaire, L.; Legare, P.; Holl, Y.; Maire, G. *Solid State Commun.* **1979**, *32*, 157–160.
(56) Wagner, C. D.; Riggs, W. M.; Davis, L. E.; Moulder, J. F.; Muilenberg, G. E. *Handbook of X-ray Photoelectron Spectroscopy*; Physical Electronics Division, Perkin-Elmer Corp.: Eden Prairie, MN, 1979.
(57) Weightman, P.; Andrews, P. T. *J. Phys. C: Solid State Phys.* **1980**, *13*, L815−L819.
(58) Weightman, P.; Andrews, P. T. *J. Phys. C: Solid State Phys.* **1980**, *13*, L821−L825.
(59) Nefedov, V. I.; Zakharova, I. A.; Moiseev, I. I.; Porai-koshits, M. A.; Vargoftik, M. N.; Belov, A. P. *Zh. Neorg. Khim.* **1973**, *18*, 3264–3268.
(60) Nefedov, V. I.; Kokunov, Y. V.; Buslaev, Y. A.; Poraikos, Ma.; Gustyako, Mp.; Ilin, E. G. *Zh. Neorg. Khim.* **1973**, *18*, 931–934.
(61) Choudary, B. M.; Kumar, K. R.; Jamil, Z.; Thyagarajan, G. *J. Chem. Soc., Chem. Commun.* **1985**, 931–932.
(62) Sakurada, O.; Takahashi, H.; Taga, M. *Bunseki Kagaku* **1989**, *38*, 407–412.
(63) Datye, A. K.; Bravo, J.; Nelson, T. R.; Atanasova, P.; Lyubovsky, M.; Pfefferle, L. *Appl. Catal., A* **2000**, *198*, 179–196.
(64) Bazzicalupi, C.; Bencini, A.; Bianchi, A.; Giorgi, C.; Valtancoli, B. *Coord. Chem. Rev.* **1999**, *184*, 243–270.
(65) Ouchene, M., S. C.; Belin, E.; Gheorghiu, A.; Theye, M. *J. Non-Cryst. Solids* **1983**, *59&60*, 625–628.
(66) Bertrand, P. A. *J. Vac. Sci. Technol.* **1981**, *18*, 28–33.
(67) Kazmerski, L. L.; Jamjoum, O.; Ireland, P. J.; Deb, S. K.; Mickelsen, R. A.; Chen, W. *J. Vac. Sci. Technol.* **1981**, *19*, 467–471.
(68) Sen, P.; Hegde, M. S.; Rao, C. N. *Appl. Surf. Sci.* **1982**, *10*, 63.
(69) Wagner, C. D. *Discuss. Faraday Soc.* **1975**, *60*, 291.
(70) Fan, J. C. C.; Goodenough, J. B. *J. Appl. Phys.* **1977**, *48*, 3524–3531.
(71) Lin, A. W. C.; Armstrong, N. R.; Kuwana, T. *Anal. Chem.* **1977**, *49*, 1228–1235.
(72) Clark, D. T.; Fok, T.; Roberts, G. G.; Sykes, R. W. *Thin Solid Films* **1980**, *70*, 261–283.
(73) Cahen, D.; Ireland, P. J.; Kazmerski, L. L.; Thiel, F. A. *J. Appl. Phys.* **1985**, *57*, 4761–4771.
(74) Hewitt, R. W.; Winograd, N. *J. Appl. Phys.* **1980**, *51*, 2620–2624.
(75) Faur, M.; Faur, M.; Jayne, D. T.; Goradia, M.; Goradia, C. *Surf. Interface Anal.* **1990**, *15*, 641–650.
(76) Tahar, R. B. H.; Ban, T.; Ohya, Y.; Takahashi, Y. *J. Appl. Phys.* **1997**, *82*, 865–870.

CG800856M